# Facile Preparation of Nickel Ferrite Nanocrystals via a Novel Reduction–Oxidation Route

Zhijun Gu, Guoli Fan, Lan Yang, Xu Xiang, Shubin Liu, and Feng Li*
*State Key Laboratory of Chemical Resource Engineering, Beijing University of Chemical Technology, Beijing 100029, P. R. China*

(Received June 23, 2008; CL-080630)

Nickel ferrite nanocrystals with narrow distribution of crystallite sizes have been obtained through a novel and facile reduction–oxidation approach. The as-prepared samples with the stoichiometric and nanocrystalline nature exhibit a promising superparamagnetic behavior.

Recently, interest in magnetic ferrite nanocrystals has greatly increased because of their importance in understanding the fundamentals in nanomagnetism and their extensive use in high-density data storage, ferrofluid technology, magnetocaloric refrigeration, magnetic resonance imaging, and heterogeneous catalysis.[1] Among those ferrites, nickel ferrite, which is a typical soft ferromagnetic material with a completely inverse spinel structure, has a large number of applications in inductors, memory cores, high frequency transformers, and recording tapes owing to its low eddy current loss and high electrochemical stability.[2] At present, several preparation techniques for nickel ferrite nanomaterials have been developed including coprecipitation,[3] reverse micelle technique,[4] sol–gel processing,[5] hydrothermal synthesis,[6] mechanical milling,[7] and combustion method.[8] However, in most cases, they require handling of large amounts of organic salts, solvents, or surfactants, which usually raises costs as well as environmental pollution, and, therefore, they are not suitable for large-scale industrial application. To overcome these problems, herein, we developed a new production strategy for nickel ferrite nanocrystals, which involves a very rapid mixing of metal cations with reducing agent and simultaneous nucleation of metallic nickel and iron within a very short time in the colloid mill process, followed by a slow oxidation in a separate hydrothermal process. This approach greatly enlarges the practical application areas of ferrite nanomaterials, since it does not require either the decomposition of complicated organic–metal compound precursors or a large amount of specialized surfactant templates.

In a typical preparation of $NiFe_2O_4$ nanocrystals, two separate solutions were prepared primarily. Solution A: analytical-grade $Ni(NO_3)_2 \cdot 6H_2O$ and $Fe(NO_3)_3 \cdot 9H_2O$ were dissolved in 50 mL of deionized water to give a solution with the $Ni^{2+}$/$Fe^{3+}$ molar ratio of 0.5. Different concentrations of initial metal ions (0.1 and 0.3 M) were used. Solution B: Sodium borohydride was dissolved in 50 mL of deionized water to form another solution with a $[NaBH_4]/([Ni^{2+}] + [Fe^{3+}])$ molar ratio of 2.0. Solutions A and B were simultaneously added rapidly to a colloid mill with the rotor speed set at around 6000 rpm and mixed over 2 min. Then the resulting slurry was transferred to 100 mL of a Teflon-lined autoclave and heated at 120 °C for 12 h. The suspension was washed with deionized water several times and then with ethanol. The solid obtained was dried at 60 °C for 12 h.

The powder X-ray diffraction (XRD) patterns of the samples are presented in Figure 1. All diffraction peaks can be indexed

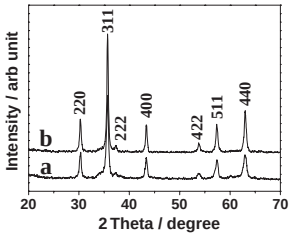


**Figure 1.** XRD patterns for $NiFe_2O_4$ synthesized by using different concentration of initial metal cations (a) 0.1 and (b) 0.3 M.

in a simple cubic lattice, and the positions along with relative intensity of peaks match well with the standard $NiFe_2O_4$ powder diffraction data (JCPDS 89-4927), which indicates the products have a *Fd3m* cubic spinel structure. The lengths of the *a* axis for the initial metal ion concentrations of 0.1 and 0.3 M are determined as 0.8344 and 0.8338 nm, respectively, consistent with that of the bulk $NiFe_2O_4$ spinel phase (0.8337 nm). Based on the Scherrer equation,[9] the average crystallite sizes of these samples are calculated as ca. 13.0 and 22.0 nm, respectively, indicative of the formation of nanoparticles. Elemental analysis by an inductively coupled plasma emission spectrometer (ICP-ES) gives a Ni/Fe atomic ratio of 0.50–0.51 in the samples, further confirming that these samples are indeed nickel ferrite with the chemical formula of $NiFe_2O_4$.

Transmission electron microscopy (TEM) analysis (Figures 2a and 2b) reveals that the $NiFe_2O_4$ samples exhibit a compact arrangement of homogeneous nanoparticles. In addition, the average crystallite sizes (from the counting of about 100 particles) are $14 \pm 4$ and $24 \pm 5$ nm, respectively, in accord with the XRD results. The consistency of crystallite sizes inferred from XRD and those observed by TEM indicates that each individual $NiFe_2O_4$ nanoparticle can be considered as a single crystal. A typical high-resolution TEM image of an individual $NiFe_2O_4$ crystallite (Figure 2c) along with a selected area electron diffraction (SAED) for $NiFe_2O_4$ sample of 14-nm size indicates interplanar distances of 0.251 nm that are characteristic of (311) $NiFe_2O_4$ spinel planes. In addition, energy dispersive X-ray spectroscopy (EDX) analysis on the $NiFe_2O_4$ sample (Figure 2d) shows that the sample contains desired Ni and Fe elements and that the atomic ratio of Ni/Fe is 2:1, in agreement with the above ICP analysis. The above results are consistent with the nanocrystalline and stoichiometric nature of the obtained ferrite nanoparticles. The temperature dependence of magnetization of nickel ferrites was measured using a superconducting quantum interference device (SQUID) magnetometer from 5 to 400 K at an applied field of 100 Oe, as shown in Figure 3a. Clearly, the temperature-dependent magnetization of the $NiFe_2O_4$ ferrites is greatly different between the zero-field-cooling (ZFC) and field-cooling (FC) measurements. The

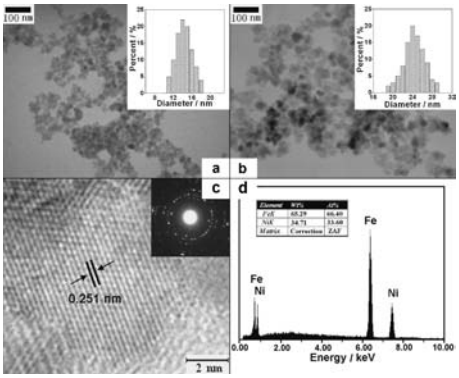


**Figure 2.** TEM images for $NiFe_2O_4$ of 14- (a) and 24-nm size (b), along with HRTEM image (c) and EDX pattern (d) for ferrite sample of 14-nm size (The insects are the distribution of particle sizes and SAED pattern.).

ZFC magnetization increases as the temperature rises from 5 K and decreases after reaching a maximum at 190 K for ferrite of 14-nm size and 290 K for that of 24-nm size, which is the blocking temperature ($T_B$) at which the thermal energy is comparable to the energy barrier of magnetic anisotropy for spin reorientation.[10] In a FC curve, the magnetization having a maximum at 5 K steadily decreases with increasing temperature and starts to overlap with ZFC curve above $T_B$. The temperature-dependent decay of magnetization for 14-nm sample (Figure 3c) shows that the sample becomes demagnetized when the temperature rises above $T_B$, suggesting that the sample has gone through a superparamagnetic relaxation process.[11] The larger 24-nm sample needs more thermal energy to get over the energy barrier and thus shows a higher $T_B$ than 14-nm spinel.[12]

The room-temperature magnetization curves and hysteresis loops of nanoparticles are shown in Figure 3b. Clearly, the samples show a room-temperature superparamagnetism with near-zero coercivity and remanence,[13] due to their lower energy barrier of magnetic anisotropy of nanomaterials. The measured saturation magnetization for 14- and 24-nm ferrite samples are 30.8 and 41.6 emu/g, respectively, which are smaller than that for the bulk nickel ferrite (55 emu/g).[14] A decrease in saturation magnetization with the crystallite size is proposed mainly to the

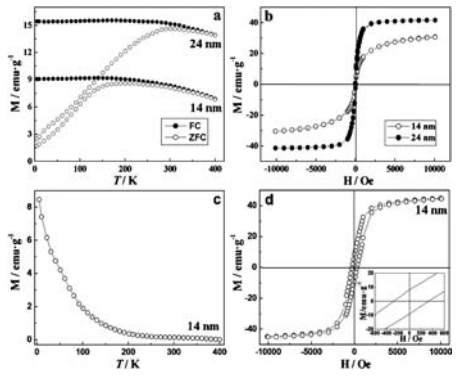


**Figure 3.** (a) Temperature dependence of magnetization for zero-field-cooled (ZFC) and field-cooled (FC) at an applied field of 100 Oe and (b) room-temperature hysteresis loops for $NiFe_2O_4$ ferrites; (c) temperature dependence of magnetization decay cooled under a magnetic field of 100 Oe and (d) hysteresis loop at 5 K for 14-nm $NeFe_2O_4$.

larger surface spin canting and surface disorder of the smaller magnetic nanoparticles.[15] Meanwhile, the presence of a magnetic dead or antiferromagnetic layer on the surface of small nanoparticles is also probably an origin of magnetization decrease.[16] At 5 K, 14-nm $NiFe_2O_4$ shows higher saturation magnetization and coercivity (Figure 3d).

In the present system, the mixing of $Ni^{2+}$ and $Fe^{3+}$ cations with reducing agent and nucleation of metals are completed within a very short time in the vigorously stirring colloid mill. Thus, nucleation and nuclei growth taking place simultaneously can be avoided, which facilitates nuclei with a narrow range of particle sizes.[17] On the other hand, the reduction takes place in a thin liquid film under conditions of high-speed fluid shear and high pressures and friction between the stator and rotor (rotating at 6000 rpm) with the mixture also being subjected to intensive vibration. In this highly turbulent zone, the newly formed metal nuclei undergo energetic collisions and this, together with the large hydraulic shear forces to which the nucleation mixture is subjected, implying that agglomeration of the nuclei is inhibited and their size remains at a minimum. The metal nuclei were then oxidized by the trace amounts of dissolved oxygen to corresponding $Ni(OH)_2$ and $Fe(OH)_3$ compounds in the hydrothermal process. At last, through the structural transformation, $NiFe_2O_4$ nanocrystals with the uniform crystallite sizes and high stoichiometry were achieved.

The present study provides an effective, environmentally benign approach for the preparation of nickel ferrite nanocrystals with narrow distribution in crystallite size. Further work on the synthesis of a range of ferrite spinels of commercial importance such as (Co, Mn, Cu, and Zn) ferrite materials is currently underway in our laboratory.

## References

1 T. Tsuchiya, H. Yamashiro, T. Sei, T. Inamura, *J. Mater. Sci.* **1992**, *27*, 3645.
2 Z. H. Zhou, J. M. Xue, J. Wang, H. S. O. Chan, T. Yu, Z. X. Shen, *J. Appl. Phys.* **2002**, *91*, 6015.
3 A. S. Albuquerque, J. D. Ardisson, W. A. A. Macedo, J. L. López, R. Paniago, A. I. C. Persiano, *J. Magn. Magn. Mater.* **2001**, *226–230*, 1379.
4 A. Kale, S. Gubbala, R. D. K. Misra, *J. Magn. Magn. Mater.* **2004**, *277*, 350.
5 J. H. Liu, L. Wang, F. S. Li, *J. Mater. Sci.* **2005**, *40*, 2573.
6 Y. Cheng, Y. Zheng, Y. Wang, F. Bao, Y. Qin, *J. Solid State Chem.* **2005**, *178*, 2394.
7 Y. T. Pavlyukhin, Y. Y. Medikov, V. V. Boldyrev, *J. Solid State Chem.* **1984**, *53*, 155.
8 S. Vivekanandhan, M. Venkateswarlu, N. Satyanarayana, *Mater. Lett.* **2004**, *58*, 2717.
9 N. C. Pramanik, T. Fujii, M. Nakanishi, J. Takada, *J. Mater. Chem.* **2004**, *14*, 3328.
10 E. Kang, J. Park, Y. Hwang, M. Kang, J.-G. Park, T. Hyeon, *J. Phys. Chem. B* **2004**, *108*, 13932.
11 A. J. Rondinone, C. Liu, Z. J. Zhang, *J. Phys. Chem. B* **2001**, *105*, 7967.
12 A. J. Rondinone, A. C. S. Samia, Z. J. Zhang, *J. Phys. Chem. B* **1999**, *103*, 6876.
13 S.-H. Yu, M. Yoshimura, *Chem. Mater.* **2000**, *12*, 3805.
14 H. Nathani, S. Gubbala, R. D. K. Misra, *Mater. Sci. Eng., B* **2005**, *121*, 126.
15 C. Yao, Q. Zeng, G. F. Goya, T. Torres, J. Liu, H. Wu, M. Ge, Y. Zeng, Y. W. Wang, J. Z. Jiang, *J. Phys. Chem. C* **2007**, *111*, 12274.
16 N. Bao, L. Shen, Y. Wang, P. Padhan, A. Gupta, *J. Am. Chem. Soc.* **2007**, *129*, 12374.
17 Y. Zhao, F. Li, R. Zhang, D. G. Evans, X. Duan, *Chem. Mater.* **2002**, *14*, 4286.

Published on the web (Advance View) August 9, 2008; doi:10.1246/cl.2008.968